A successful comparison between a non-invasive measurement of local profiles during drying of a highly shrinkable food material (eggplant) and the spatial reaction engineering approach

Putranto, A., & Chen, X. D. (2018). A successful comparison between a non-invasive measurement of local profiles during drying of a highly shrinkable food material (eggplant) and the spatial reaction engineering approach. *Journal of Food Engineering*, *235*, 23-31. https://doi.org/10.1016/j.jfoodeng.2018.04.024

Published in:
Journal of Food Engineering

Document Version:
Peer reviewed version

Queen's University Belfast - Research Portal:
Link to publication record in Queen's University Belfast Research Portal

Publisher rights
Copyright 2018 Elsevier. This manuscript is distributed under a Creative Commons Attribution-NonCommercial-NoDerivs License (https://creativecommons.org/licenses/by-nc-nd/4.0/), which permits distribution and reproduction for non-commercial purposes, provided the author and source are cited.

General rights
Copyright for the publications made accessible via the Queen's University Belfast Research Portal is retained by the author(s) and / or other copyright owners and it is a condition of accessing these publications that users recognise and abide by the legal requirements associated with these rights.

Take down policy
The Research Portal is Queen's institutional repository that provides access to Queen's research output. Every effort has been made to ensure that content in the Research Portal does not infringe any person's rights, or applicable UK laws. If you discover content in the Research Portal that you believe breaches copyright or violates any law, please contact openaccess@qub.ac.uk.

Download date:16. Jun. 2021

A successful comparison between a non-invasive measurement of local profiles during drying of a highly shrinkable food material (eggplant) and the spatial reaction engineering approach

Abbreviated running title:

Modeling local profiles inside of food materials by the spatial reaction engineering approach

Aditya Putranto[1]**, Xiao Dong Chen[2]*

[1]School of Chemistry and Chemical Engineering, Queen's University Belfast, David Keir Building, Stranmilis Road, Belfast BT9 5AG, United Kingdom

[2]School of Chemical and Environmental Engineering, College of Chemistry, Chemical Engineering and Materials Science, Soochow University, Suzhou, Jiangsu Province, PR China

Abstract

A reliable mathematical model is useful for predicting the internal profiles inside the materials during drying.In this study, for the first time, the spatial reaction engineering approach (S-REA) is used to model the local profiles of food materials during drying. The REA is applied as the local rate of phase change and combined with a set of equations of conservation of heat and mass transfer to yield the spatial temperature and concentration profiles during drying. The S-REA predictions are benchmarked against the Magnetic Resonance Imaging (MRI) data. The study indicates that the S-REA is applicable to model the internal profiles inside food materials during drying. The S-REA predictions also show closer agreement towards the experimental data than the effective diffusion model. While the S-REA predictions are accurate, it requires minimum number of experiments to generate the drying parameters. The S-REA has contributed to better analysis of transport phenomena inside food materials during drying through generation of local profiles. The S-REA predictions are useful to interpret the sensory and quality matters during drying such as hardness and crispiness.

Key words: drying, internal profiles, model, heat and mass transfer, spatial reaction engineering approach

---

Corresponding authors' emails: *Professor Xiao Dong Chen (xdchen@mail.suda.edu.cn), ** Dr. Aditya Putranto (a.putranto@qub.ac.uk)

1. Introduction

Drying is commonly employed in food and bioproduct processing to remove moisture to extend the shelf life and to minimise transportation costs (Chou et al., 2000). It is an energy intensive process since large amount of heat needs to be supplied for vaporising water. Drying may also alter the product structure, impacting on the quality. For fruits and vegetables, drying may lead to non-enzymatic browning, loss of ascorbic acid, loss of beta carotene content, color changes and many other chemical changes (Pan et al., 1999; Cnossen et al., 2002).

Tailoring drying schemes and conditions are feasible to ensure good product quality is met. The internal profiles of moisture content and temperature along with the microstructures are essential information. This understanding is useful to systematically fine-tune the drying schemes. The ability to manage average moisture content and average temperature seems not sufficient these days. The antioxidant capacity, phenolic content, loss of vitamin C and color changes during drying of fruits and vegetables can be related to the local moisture content and the local temperature (Fan et al., 2017; Horuz et al., 2017). For rice, high temperature and moisture content gradients may induce fissuring and breakage. Drying under time-varying conditions has shown to minimise the fissuring since it allows the moisture and heat to equilibrate inside the samples (Aqueretta et al., 2007; Dong et al., 2010). In baking, the understanding of local variables assists in optimising crispness, softness and color changes due to browning reactions, starch gelatinisation and protein denaturation (Hadiyanto et al., 2008). Since evaporation/condensation occurs inside bread, the temperature gradients inside the samples need to be studied (De Vries et al., 1989).

Reliable drying models can be used assist in predicting the internal profiles during drying. For this purpose, the spatial drying models are useful. The diffusion-based models are commonly implemented to describe drying with a wide range of accuracy is shown (Vaquiro

et al., 2009; Brasiello et al., 2013; 2017). Most of the models use the effective diffusivity to lump the capillary and water vapor diffusivity (Mariani et al., 2007; Vaquiro et al., 2009; Brasiello et al., 2011; 2017). In addition, Luikov's based models (Luikov, 1975) based on classical thermodynamics are used to represent the spatial profiles. The models postulate that the thermal and moisture potential gradient within a porous body cause the vapor and liquid water transfer so that the flux of liquid water and water vapor is proportional to the thermal gradient and moisture potential gradient. The two-way coupled system of Luikov's approach was implemented to model timber drying and a reasonable agreement towards the experimental data is shown (Thomas et al., 1980; Kulasiri and Samarasinghe, 1986). Similarly, Whitaker's approach (Whitaker, 1977) can be implemented to generate the spatial profiles during drying. Darcy's law is usually used to describe the momentum transfer in liquid and gas phases while the mass transfer considers capillary action as well as evaporation/condensation. This approach has been used to model several drying process well (Hager et al., 2000; Torres et al., 2011).

The reaction engineering approach (REA) is basically a 'middle-path' approach to model drying. The major physics of drying is captured by the relative activation energy of the REA. The relative activation energy is essentially material characteristics which describe the difficulty to remove moisture from materials being dried. At the beginning of drying, the relative activation energy is zero and it keeps increasing as drying progresses. When the equilibrium condition is achieved, the relative activation energy is one. The REA requires minimum number of experiments to generate the relative activation energy since the one generated from one accurate drying run is applicable to project drying the same materials at other conditions provided the similar initial moisture content (Chen and Putranto, 2013). When compared to characteristics drying rate curve (CDRC), the REA gives advantages in yielding natural transition during drying since it does not depend on the critical moisture content (Baini

and Langrish, 2007). Therefore, it is applicable to describe the heat and mass transfer processes under time-varying conditions (Putranto et al, 2011[a-c]). Benchmarks against diffusion-based models also showed that the REA result in closer agreement towards experimental data (Putranto and Chen, 2011[a-b]).

The REA in its lumped format is further called as the lumped reaction engineering approach (L-REA) and it has been combined with a set of equations of conservation of heat and mass transfer to yield a spatial model labelled as the spatial reaction engineering approach (S-REA) (Chen and Putranto, 2013). The S-REA is non-equilibrium multiphase model in whichthe REA is used as the local evaporation/condensation rate. The use of non-equilibrium multiphase model is suggested as it is more general and can be used to assess the applicability of the equilibrium multiphase drying model (Zhang and Datta, 2004; Chen, 2007). It also yields better understanding of transport phenomena during drying since the profiles of concentration of water vapor can be established. In S-REA, the moisture content inside the solid matrix is not assumed to be in equilibrium with the concentration of water vapor inside pore spaces. The S-REA has been used so far to describe a number of heat and mass transfer processes including convective drying, intermittent drying, baking and water vapor sorption (Putranto and Chen, 2015[a-c]). In these studies, the S-REA is shown to be able to model well the average moisture content.

However, it is not certain whether the S-REA can be used to model the internal profiles inside food materials during drying. In this study, for the first time, the S-REA is applied to model the local profiles during drying. The capability of the S-REA is tested by benchmarking the S-REA predictions against a set of Magnetic Resonance Imaging (MRI) data. The eggplant is chosen as a shrinkable vegetable that present reasonable challenges to model. The outline of

this paper is as follows. The experimental details are reviewed briefly followed by the mathematical modelling using S-REA. The reported results of modelling are then discussed.

2. Review of experimental details

The experimental data for validating the results of modelling are derived from previous study (Brasiello et al., 2017). For better understanding of the modelling, the experimental details are reviewed briefly here. The fresh eggplant is firstly stored in the fridge at 4 °C before processing. The samples are then washed, cut longitudinally around the centre from left to right and shaped using a steel mould to give an initial diameter of 2 cm. The samples are randomised before processing to avoid unavoidable difference in material structure. The initial sample moisture content is 12.75± 0.96 kg water.kg dry solids^{-1} (Brasiello et al., 2017). Drying is conducted in a forced convective dryer (Espec Corp SU221) at drying air temperature of 50 °C and air velocity of 1.2 m.s^{-1}. During drying, the weight loss is measured at particular timings using gravimetric method and the moisture content is analysed using the AOAC standards (Helrich, 1990). For the measurement of the internal moisture content distribution at different timings, Magnetic Resonance Imaging (MRI) is implemented (Brasiello et al., 2017).

3. Mathematical modelling using the spatial reaction engineering approach (S-REA)

The spatial reaction engineering approach (S-REA) is used to model the convective drying of eggplant in this study. The details of the reaction engineering approach (REA) have been published previously (Chen and Putranto, 2013; Putranto and Chen, 2015[a,b]; 2016; Putranto et al., 2017). The S-REA consists of a set of equations of conservation of heat and mass transfer in which the REA is used to describe the local evaporation rate. In S-REA, the moisture content inside the solid matrix is not assumed to be in equilibrium with the

concentration of water vapor inside pore spaces. The REA serves as a source and depletion term for equation of conservation of water vapour and liquid water, respectively.

The mass balance of liquid water can be represented as (Chen and Putranto, 2013; Putranto and Chen, 2015[a-c]):

$$\frac{\partial(C_s X)}{\partial t} = \frac{1}{r}\frac{\partial}{\partial r}(D_w r \frac{\partial(C_s X)}{\partial r}) - \dot{I} \quad (1)$$

where t is the time (s), r is the sample radius (m), X is the concentration of liquid water (kg H_2O kg dry solids^{-1}), D_w is the capillary diffusivity (m^2 s^{-1}),C_s is the solids concentration (kg dry solids m^{-3}), $\dot{I}$ is the local evaporation or condensation rate (kgm^{-3}s^{-1}) and $\dot{I}$is >0 when evaporation occurs locally.

The mass balance of water vapor can be written as (Chen and Putranto, 2013; Putranto and Chen, 2015[a-c]):

$$\frac{\partial C_v}{\partial t} = \frac{1}{r}\frac{\partial}{\partial r}(D_v r \frac{\partial C_v}{\partial r}) + \dot{I} \quad (2)$$

where C_v is the concentration of water vapor (kg H_2O m^{-3}) and D_v is the water vapor diffusivity (m^2 s^{-1}).

In addition the heat balance can be represented as (Chen and Putranto, 2013; Putranto and Chen, 2015[a-c]):

$$\rho C_p \frac{\partial T}{\partial t} = \frac{1}{r}\frac{\partial}{\partial r}(kr \frac{\partial T}{\partial r}) - \dot{I}\,\Delta H_v \quad (3)$$

where T is the sample temperature (K). ρ is the sample density (kg m^{-3}), $C_p$is the sample specific heat capacity (J kg^{-1} K^{-1}), ΔH_v is the water vaporization enthalpy (J kg^{-1}) and k is the sample thermal conductivity (W m^{-1} K^{-1}).

The initial and boundary conditions of equations (1) to (3) are:

$t=0$, $X=X_o$, $C_v=C_{vo}$, $T=T_o$ (initial condition, uniform initial concentrations and temperature) (4)

$r=0,, \frac{dX}{dr}=0\ , \frac{dC_v}{dr}=0\ , \frac{dT}{dr}=0$ (symmetrical condition) (5)

$r=R,$

$$-C_s D_w \frac{dX}{dr} = h_m \varepsilon_w (\frac{C_{v,s}}{\varepsilon} - \rho_{v,b})$$ (convective boundary for liquid water transfer) (6)

where ε_w is the fraction of surface area covered by liquid water.

$$-D_v \frac{dC_v}{dr} = h_m \varepsilon_v (\frac{C_{v,s}}{\varepsilon} - \rho_{v,b})$$ (convective boundary for water vapor transfer) (7)

where ε_v is the fraction of surface area covered by water vapor.

$$k \frac{dT}{dr} = h(T_b - T)$$ (convective boundary for heat transfer) (8)

$\dot{I}$ is the local drying or wetting rate within the solid structure described as (Putranto and Chen, 2015[a-c]):

$$\dot{I} = h_{m_{in}} A_{in} (C_{v,s} - C_v)$$ (9)

where $h_{m,in}$ is the internal mass transfer coefficient (m s^{-1}), A_{in} is the total internal surface area available for phase change ($m^2 m^{-3}$), $C_{v,s}$ is the internal-solid-surface water vapor concentration (kg m^{-3}).

By implementing the REA, internal-surface water vapor concentration can be written as (Chen and Putranto, 2013):

$$C_{v,s} = \exp(\frac{-\Delta E_v}{RT}) C_{v,sat} \quad (10)$$

where ΔE_v is the activation energy (J mol^{-1} K^{-1}) and $C_{v,sat}$ is the internal-saturated water vapour concentration (kg m^{-3})

Therefore, the local drying or wetting rate can be expressed as (Chen and Putranto, 2013):

$$\dot{I} = h_{m_{in}} A_{in} (\exp(\frac{-\Delta E_v}{RT}) C_{v,sat} - C_v) \quad (11)$$

The relative activation energy of convective drying of eggplant, as fingerprint of the REA, is established from eggplant drying at drying air temperature of 60 °C (Adiletta et al, 2014). Only one temperature data set is used to generate the relate activation energy function. Based on the experimental data set of drying at 60 °C, the activation energy is calculated. Dividing the activation energy (ΔE_v) with the equilibrium activation energy ($\Delta E_{v,b}$) yields the relative activation energy ($\Delta E_v/\Delta E_{v,b}$). The detailed equations to evaluate the activation energy and equilibrium activation energy have been presented previously (Putranto and Chen, 2015[s-c]). The relationship between the relative activation energy and average moisture content can be represented by simplified mathematical equation obtained by least square method. The relative activation energy ($\Delta E_v/\Delta E_{v,b}$) of eggplant during convective drying can be represented as:

$$\frac{\Delta E_v}{\Delta E_{v,b}} = -7.69\times10^{-4}(\overline{X} - X_b)^3 + 2.32\times10^{-2}(\overline{X} - X_b)^2 - 2.48\times10^{-1}(\overline{X} - X_b) + 1 \quad (12)$$

The good agreement between the fitted and experimental relative activation energy is shown by R^2 of 0.999 and plotted in Figure 1. The format of equation (12) can be varied to be the best

213 fit but in this case, equation (12) is sufficient to describe the relative activation energy of
214 eggplant.

215

216 For modelling using S-REA, equation (12) is implemented to describe the 'local'
217 relative activation energy by substituting the average moisture content ($\overline{X}$) with the local
218 moisture content (X). This is to say that the kinetics obtained for average parameters can also
219 be used as the local kinetics. Combining the 'local' relative activation energy with the
220 equilibrium activation energy results in the 'local' activation energy which represents the
221 'local' behavioural changes of eggplant as affected by the local variables and structures. The
222 'local' activation energy is then implemented to represent the local evaporation and
223 condensation rate shown in equation (11). The determination of transport properties used in the
224 modelling is presented in Appendix A while the calculation of internal surface area (A_{in}) is
225 shown in Appendix B.

226

227 In order to yield the spatial profiles of moisture content, concentration of water vapor
228 and temperature, equations (1) to (3) are solved simultaneously in conjunction with the initial
229 and boundary conditions (equations (4) to (8)) as well as the relative and equilibrium activation
230 energy. Matlab® is used to solve the equations simultaneously and the results of modelling are
231 validated towards the Magnetic Resonance Imaging (MRI) data of convective drying of
232 eggplant at drying air temperature of 50 °C.

233

234 **4. Results and Discussion**

235 Figure 2 indicates the average moisture content during drying modelled by the S-REA.
236 A very good agreement with the experimental data is resulted by the modelling. It is further

237 confirmed by R^2 of 0.999. When benchmarking against the diffusion-based model (Brasiello
238 et al., 2017), the S-REA results in closer agreement with experimental data. The diffusion-
239 based model gives $R^2$of 0.92 (Brasiello et al., 2017). This indicates that the S-REA describes
240 accurately the average moisture content during drying. The applicability of the S-REA may be
241 because the relative activation energy is accurate to represent the structural changes inside the
242 eggplant samples during drying.
243
244 The distribution of moisture content inside the samples at drying time of 1800s is shown
245 in Figure 3. The S-REA predicts accurately the spatial profiles of moisture content at this initial
246 drying period. At the sample edge, the moisture content is lower than that at the core since the
247 moisture is transferred from the centre to the drying air via convection. This also indicates that
248 the moisture migrates outwards during drying. Although the modelling implemented by
249 Brasiello et al. (2017) represents the parabolic profiles, the other model seems to overestimate
250 the drying rate.
251
252 For drying time of 3600 s, the spatial profiles of moisture content inside the eggplant
253 samples are represented in Figure 4. Similar to Figure 3, the S-REA predictions match well
254 with the experimental data and confirmed by R^2 of 0.98. As drying progresses, the moisture
255 content at this drying period is lower than that at 3600 s. Similar to the profiles at drying time
256 of 1800 s, the maximum moisture content is located at the centre of the eggplant samples. Both
257 the MRI data and the S-REA show the similar behaviors. The other model (Brasiello et al.,
258 2017) shows the lower predictions of the moisture content at this drying time.
259
260 Figure 5 shows the distribution of moisture content at drying time of 5400 s. The S-
261 REA also represents accurately the internal profiles of moisture content at this drying period.

Compared to the modelling by the other modelling, a better agreement towards the experimental data is shown by the S-REA. Similar results are also found during drying at drying time of 7200 s as indicated in Figure 6. As drying progresses, the gradient of moisture content inside the eggplant samples decreases in line with the depletion of moisture inside the samples.

As a whole, the S-REA outlined in this paper has performed very well in predicting the local behaviour of moisture transfer. It is in fact quite precise, which is a nice surprise considering it is based on the lumped model to obtain the kinetics data. For better representation of transport processes inside the materials, the spatial concentration of water vapor during drying time is generated and shown in Figure 7. At the beginning of drying, the distribution of concentration of water vapor is not large but this increases until drying time of 8000s. More plateau-like profiles are then observed in the later drying period. This seems to correspond well with a relatively uniform moisture content and temperature profiles. The maximum concentration of water vapor is attained at the sample core which may be due to the maximum local moisture content at this location. The water vapor at the sample core diffuses outwards during drying since the concentration of water vapor in the drying air is lower than that at the sample surface.

Figure 8 indicates the spatial profiles of the local evaporation rate during drying inside the eggplant samples. At the beginning of drying, the local evaporation rate seems to be relatively uniform although the moisture content at the sample core is higher. The initial porosity of the samples is 0.72. As drying progresses, the local evaporation rate at the inner part becomes higher than that that at the outer part which may bedue to the higher local pore surface relative humidity at the inner part of the samples as shown in Figure 9. The higher

moisture content at the core of the samples as indicated in Figure 2 to 5 seems to correspond to this condition. This also corresponds to the profiles of water vapour concentration as shown in Figure 7. Along drying, the local evaporation rate increases because of the increase of temperature. Nevertheless, this only lasts until drying time of 5000 s. After this period, the moisture content inside the samples decreases and the equilibrium condition is approached. The gradient of local evaporation rate also decreases towards the end of drying. In agreement with this, as shown in Figure 10, the local pore surface relative humidity inside the samples decreases as drying progresses. It has been shown here that the REA serves well as the local evaporation rate.

The spatial temperature profiles during drying are shown in Figure 10. The sample temperature increases as moisture being reduced to approach to the drying air temperature. The temperature at the outer part of the eggplant sample is slightly higher than that at the sample core. This is reasonable since the sample receives heat from the surrounding and the heat is mostly used for vaporizing the moisture. Any heat left is then penetrated inwards via conduction to increase the sample temperature. Nevertheless, the gradient temperature inside the eggplant samples is essentially small which is also indicated by *Ch_Bi*(Chen and Peng, 2005) which is found to be about 0.002. The low gradients of temperature during drying of food materials are also reported previously (Putranto and Chen, 2015[a-c]; Putranto et al., 2017). As drying progresses, the temperature gradient actually decreases and no noticeable of temperature difference is observed at the end of drying. This is in line with plateau profiles of moisture content, concentration of water vapor and local evaporation rate at the end of drying as discussed above. No temperature profiles are published by the other model (Brasiello et al., 2017).

In this study, the S-REA has been shown to be able to model the internal profiles of eggplant during drying. The capability is probably because of the accuracy of 'local' activation energy, resulted from combination of both 'local' relative and equilibrium activation energy. The 'local' activation energy seems to be flexible to represent the 'local' drying behaviours at micro-scale as affected by local structure and drying conditions. As the local evaporation rate, the REA is useful not only to link equations of conservation of liquid water and water vapor but also to interpret the complex interrelationships of moisture content, concentration of water vapor and temperature during drying.

Since the S-REA is applicable to model the internal profiles of food materials during drying, the S-REA can be implemented to evaluate the local mechanical properties. These predictions are useful to interpret the sensory and quality matters such as hardness and crispiness. These sensory properties cannot yet be predicted even with the most comprehensive models (Wang et al., 2012; Kharaghani et al., 2013). In addition, it is interesting to see the S-REA applications in predicting the local profiles of more challenging drying cases including intermittent drying, infrared-heating, microwave and ultrasonic-assisted drying.

Conclusions

In this study, for the first time, the S-REA is used to model the internal profiles inside food materials during drying. The REA is used as the local evaporation/condensation rate and coupled with a set of equations of conservation of heat and mass transfer. When benchmarked against the available MRI data, the S-REA shows excellent predictions. The local evaporation rate has also been plotted to provide an insight to the transport phenomena. The understanding of local profiles during drying of food materials can be gained by the S-REA. The S-REA is

readily implemented as a tool to analyse the transport phenomena inside food materials during drying. The S-REA framework can be used to fine-tune the drying schemes to yield food materials with the desirable product characteristics.

Nomenclatures

A	surface area of samples	(m^2)
A_{in}	internal surface area	(m^2 m^{-3})
A_p	cell surface area	(m^2)
C_p	specific heat of sample	(J $kg^{-1}K^{-1}$)
C_s	solids concentration	(kg m^{-3})
C_v	water vapor concentration	(kg m^{-3})
$C_{v,s}$	internal-surface vapor concentration	(kg m^{-3})
$C_{v,sat}$	internal-saturated vapor concentration	(kg m^{-3})
D_v	effective water vapor diffusivity	(m^2s^{-1})
$D_{v,o}$	water vapor diffusivity	(m^2s^{-1})
D_w	liquid diffusivity	(m^2s^{-1})
h	heat transfer coefficient	(W $m^{-2}K^{-1}$)

h_m	mass transfer coefficient	(m s^{-1})
$h_{m,in}$	internal mass transfer coefficient	(m s^{-1})
I	local evaporation/condensation rate	(kg $m^{-3}s^{-1}$)
k	thermal conductivity of sample	(W $m^{-1}K^{-1}$)
m_p	dry mass of cell	(kg)
m_s	dried mass sample of material	(kg)
m_w	mass of liquid water	(kg)
n	constant	
N	number of cell in samples	
n_p	number of cell per unit volume	(m^{-3})
r	radial position	(m)
RH_b	relative humidity of drying air	
r_p	cell radius	(m)
T	sample temperature	(K)
T_s	surface sample temperature	(K)
t	time	(s)
T_b	drying air temperature	(K)
V	volume of sample	(m^3)
V_0	initial volume of sample	(m^3)
V_p	cell volume	(m^3)
v_w	mass fraction of water	
X	moisture content on dry basis	(kg kg^{-1})
$\overline{X}$	average moisture content on dry basis	(kg kg^{-1})
X_b	equilibrium moisture content on dry basis	(kg kg^{-1})
X_o	initial moisture content	(kg kg^{-1})
ΔE_v	apparent activation energy	(J mol^{-1})
$\Delta E_{v,b}$	equilibrium activation energy	(J mol^{-1})
$\Delta E_v/\Delta E_{v,b}$	relative activation energy	
ΔH_v	vaporization enthalpy of water	(J kg^{-1})
ε	porosity	
ε_w	fraction of surface area covered by liquid water	
ε_v	fraction of surface area covered by water vapor	
ε_o	initial porosity	
ρ	sample density	(kg.m^{-3})
ρ_s	density of solids	(kg.m^{-3})
$\rho_{v,b}$	vapor concentration in drying medium	(kg. m^{-3})
$\rho_{v,s}$	surface vapor concentration	(kg.m^{-3})
$\rho_{v,sat}$	saturated vapor concentration	(kg m^{-3})
ρ_w	density of water	(kg m^{-3})
τ	turtuosity	

415

416

417

418

419

420

421

422

423

424

425

426

427

428

429

430

431

432

433 **Appendix A. The physical and transport properties used in the modeling**

434 ρ=670 kg m^{-3} (B1)

435 where ρ is the density of eggplant(kg m^{-3}) (Llave et al, 2016).

436 $C_p = 1470 + 2720X$ (B2)

437 where C_p is the specific heat of eggplant (J kg^{-1} K^{-1}) (Lamb, 1976).

438 $k = 14.8 + 49.3X$ (B3)

where k is the thermal conductivity of eggplant (W m^{-1} K^{-1}) (Sweat, 1974).

$$D_v = D_{v_o} \frac{\varepsilon}{\tau} \quad \text{(B4)}$$

where D_v is the effective water vapour diffusivity (m^2s^{-1}) (Bird et al, 2002).

$$D_{vo} = 2.09\times10^{-5} + 2.137\times10^{-7}(T - 273.15) \quad \text{(B5)}$$

where D_{vo} is the vapour diffusivity (m^2s^{-1})(Slattery and Bird, 1958).

$$\tau = \varepsilon^{-n} \quad \text{(B6)}$$

where τ is the turtuosity, ε is the porosity and n is the value between 0 to 0.5(Audu and Jeffreys, 1975).

$$C_s = \frac{1-\varepsilon}{\frac{1}{\rho_s} + \frac{X}{\rho_w}} \quad \text{(B7)}$$

where C_s is the solid concentration (kg m^{-3}), ρ_s is the solid density (kg m^{-3}) and ρ_w is the water density (Putranto and Chen, 2015[a-c]).

$$\varepsilon = 1 - \frac{V_0}{V}(1-\varepsilon_0)\left(\frac{\frac{\rho_s}{\rho_w}X + 1}{1 + \frac{\rho_s}{\rho_w}X_0}\right) \quad \text{(B8)}$$

where ε is the porosity, $V$is the sample volume (m^3) , V_0 is the initial sample volume (m^3) and X_0 is the initial moisture content (kg water kg dry $solids^{-1}$) (Madiouli et al, 2007).

$$\varepsilon_w = \frac{C_s X}{\rho_w} \quad \text{(B9)}$$

where ε_w is the fraction of surface area covered by liquid water (Ousegui et al,, 2010).

455 $$\varepsilon_v = \frac{C_v}{\rho_v} \quad \text{(B10)}$$

456 where ε_v is the fraction of surface area covered by water vapour (Ousegui et al., 2010).

457 $$D_w = 1.05 \times 10^{-4} \exp(-\frac{3265.91}{T}) \quad \text{(B11)}$$

458 where D_w is the capillary diffusivity ($m^2\ s^{-1}$) (Brasiello et al, 2017).

459 $$R = R_0(0.1817 + 0.9185\frac{X}{X_0})^{0.5} \quad \text{(B12)}$$

460 where R is the sample radius (m) and R_0 is the initial sample radius (m) (Adiletta et al, 2014).

461

462

463

464

465

466 **Appendix B. Evaluation of internal surface area (A_{in})** (Kar and Chen, 2010; Putranto and

467 Chen, 2015[a-c])

468 $$A_p = 4\pi r_p^{\ 2} \quad \text{(C1)}$$

469 where A_p is the cell surface area (m^2) and r_p is the cell diameter (m).

470 $$V_p = \frac{4}{3}\pi r_p^{\ 3} \quad \text{(C2)}$$

471 where V_p is the cell volume (m^3)

472 $$m_p = \rho_p V_p (1 - v_w) \quad \text{(C3)}$$

where m_p is the cell mass (kg) and v_w is the volume fraction of water

$$N = \frac{m_s}{m_p} \quad \text{(C4)}$$

where N is the number cell in samples and m_s is the dried mass of the samples (kg)

$$n_p = \frac{N}{V_s} \quad \text{(C5)}$$

where n_p is the number of cell per unit volume and V_s is the dried cell volume (m^3)

$$A_{in} = n_p A_p \quad \text{(B6)}$$

where A_{in} is the internal surface area (m^2 m^{-3})

References

Adiletta, G., Iannone, G., Russo, P., Patimo, G., De Pasquale, S., Di Matteo, M., 2014. Moisture migration by magnetic resonance imaging during eggplant drying: preliminary study. International Journal of Food Science and Technology 49, 2602-2609.

Aquerreta J., Iguaz A., Arroqui C., and Virseda P., 2007. Effect of high temperature drying and tempering on rough rice quality. Journal of. Food Engineering 80, 611-918.

Baini, R., Langrish, T.A.G., 2007. Choosing an Audu, T.O.K., Jeffreys, G.V. The drying of drops of particulate slurries. Trans IChemE Part A. 1975; 53: 165-175.

493 appropriate drying model for intermittent and continuous drying of bananas, Journal of Food
494 Engineering 79, 30–343.
495 Baini, R., Langrish, T.A.G., 2007. Choosing an appropriate drying model for intermittent and
496 continuous drying of bananas, Journal of Food Engineering 79, 30–343.
497 Bird, R. B., Stewart, W. E., and Lightfoot, E. N. 2002. Transport Phenomena, 2nd
498 international ed., John Wiley, New York.
499 Brasiello, A., Adiletta, G., Russo, P., Crescitelli, S., Albanese, D., Di Matteo, M., 2013.
500 Mathematical model of eggplant drying: shrinkage effect. Journal of Food
501 Engineering 114, 99-105.
502 Brasiello, A., Iannone, G, Adiletta, G., De Pasquale, S., Russo, P., Di Matteo, M., 2017.
503 Mathematical model for dehydration and shrinkage: Prediction of eggplant's MRI
504 spatial profiles. Journal of Food Engineering 203, 1-5.
505 Chen, X.D., 2007. Moisture diffusivity in food and biological materials. Drying Technology
506 25, 1203–1213.
507 Chen, X.D., Putranto, A., 2013. Modeling Drying Processes: A Reaction Engineering
508 Approach. Cambridge University Press, U.K.
509 Chen, X.D, Peng, X.F., 2005. Modified Biot number in the context of air drying of small moist
510 porous objects. Drying Technology 23, 83-103.
511 Chou, S.K., Chua, K.J., Mujumdar, A.S., Hawlader, M.N.A., Ho, J.C., 2000. On the
512 intermittent drying of an agricultural product, TransIChemE Part C 78, 193-203.
513 Cnossen, A.G., Siebenmorgen, T.J., Yang, W., 2002. The glass transition temperature
514 concept in rice drying and tempering: effect on drying rate. Trans. ASAE 45, 759–766
515 De Vries, U., Sluimer, P., Bloksma, A. H., 1989. A quantitative model for heat transport in
516 dough and crumb during baking. In Cereal Science and Technology in Sweden,
517 Proceedings of an International Symposium (pp. 174–188). Sweden: Lund University.

518 Dong, R., Lu, Z., Liu, Z., Nishiyama, Y., Cao, W., 2009. Moisture distribution in a rice kernel
519 during tempering drying, J. Food Eng. 91, 126–132.
520 Hadiyanto, D.C. Esveld, R.M. Boom, G. van Straten, A.J.B. van Boxtel, 2008. Product quality
521 driven design of bakery opertions using dynamic optimization. Journal of Food
522 Engineering 86, 399-413.
523 Helrich, K., 1990. Official Methods of Analysis of AOAC International, fifteenth
524 ed.Association of Official Analytical Chemists, Inc., Arlington, Virginia, USA.
525 Hager, J., Wimmerstedt, R., Whitaker, S., 2000. Steam drying a bed of porous spheres: Theory
526 and experiment, Chemical Engineering Science 55, 1675-1698.
527 Kar, S., Chen, X.D., 2010. Moisture transport across porcine skin: experiments and
528 implementation of diffusion-based models, International Journal of Healthcare
529 Technology and Management 11, 474-522.
530 Kharaghani, A., Kirsch, C., Metzger, T., Tsotsas, E., 2013. Micro-scale fluid model for drying
531 of highly porous aggregates. Computers and Chemical Engineering 52, 46-54.
532 Kulasiri, D., Samarasinghe, S., 1996. Modeling of heat and mass transfer of biological
533 materials: a simplified approach of materials with small dimension. Ecological
534 Modeling 86, 163-167.
535 Lamb, J., 1976. Influence of water on the thermal properties of foods. Chemical Industries
536 24, 1046-1048.
537 Llave, Y., Takemori, K., Fukuoka, M., Takemori, T., Tomita, H., Sakai, N.,
538 2016..Mathematical modeling of shrinkage deformation in eggplantundergoing
539 simultaneous heat and mass transfer during convectionovenroasting. Journal of Food
540 Engineering 178, 124-136.
541 Luikov, A.V., 1975. Systems of differential equations of heat and mass transfer in capillary-
542 porous bodies. International Journal of Heat and Mass Transfer 18, 1-14.

543 Madiouli, J., Lecomte, D., Nganya, T., Chavez, S., Sghaier, J., Sammouda, H., 2007. A
544 method for determination of porosity change from shrinkage curves of deformable
545 Materials, Drying Technology 25, 621–628.
546 Mariani, V.C., de Lima, A.G.B., Coelho, L.S.. 2008. Apparent thermal diffusivity estimation
547 of the banana during drying using inverse method. Journal of Food Engineering 85,
548 569–579.
549 Ousegui, A., Moresoli, C., Dostie, M., Marcos, B., 2010. Porous multiphase approach for
550 baking process – Explicit formulation of evaporation rate, Journal of Food Engineering
551 100, 535–544.
552 Pan, Y.K., Zhao, L.J., Dong, Z.X., Mujumdar, A.S., Kudra, T., 1999. Intermittent drying of
553 carrot in a vibrated fluid bed: effect on product quality. Drying Technology 17, 2323–
554 2340.
555 Putranto, A, Chen, X.D., Xiao, Z., Webley, P.A., 2011[b]. Intermittent drying of mango tissues:
556 implementation of the reaction engineering approach (REA). Industrial Engineering
557 Chemistry Research 50, 1089-1098.
558 Putranto, A., Chen, X.D., 2015[a]. An assessment on modeling drying processes: Equilibrium
559 multiphase model and the spatial reaction engineering approach. Chemical Engineering
560 Research and Design 94, 660-672.
561 Putranto, A., Chen, X.D., 2015[b]. Bread baking and its color kinetics modeled by the spatial
562 reaction engineering approach (S-REA). Food Research International 71, 58-67.
563 Putranto, A., Chen, X.D., 2015[c]. Spatial reaction engineering approach (S-REA): an effective
564 approach to model drying, baking and water vapor sorption process. Chemical
565 Engineering Research and Design101, 135-145.
566 Putranto, A., Chen, X.D., 2016. Drying of a system of multiple solvents: modeling by the
567 reaction engineering approach (REA). AIChE Journal62, 2144-2153.

568 Putranto, A., Chen, X.D., Webley, P.A., 2011[a], Modeling of drying of thick samples of mango
569 and apple tissues using the reaction engineering approach (REA). Drying Technology
570 29, 961-973.
571 Putranto, A., Chen, X.D., Zhou, W., 2011[c]. Modeling of baking of cake using the reaction
572 engineering approach (REA), Journal of Food Engineering 105, 306-311.
573 Putranto, A., Foerster, M., Woo., M.W., Chen, X.D., Selomulya, C., 2017. A continuum-
574 approach modelling of surface composition and ternary component distribution inside
575 low fat milk emulsions during single droplet drying. AIChE Journal 63, 2535-2545.
576 Slattery, J.C., Bird, R.B. 1958. Calculation of the diffusion coefficient of dilute gases and of
577 the self diffusion coefficient of dense gases. AIChE Journal 4, 137-142.
578 Sweat, V.E., 1974. Experimental values of thermal conductivity of selected fruits and
579 vegetables. Journal of Food Science 39, 1080-1083.
580 Thomas, H.R., Morgan, K., Lewis, R.W., 1980. A fully nonlinear analysis of heat and mass
581 transfer problems in porous bodies, International Journal of Numerical Methods
582 Engineering 15, 1381-1393.
583 Torres, S.S., Jomaa, W., Puiggali, J.R., Avramidis, S., 2011. Multiphysicsmodeling of vacuum
584 drying of wood. Applied Mathematical Modelling 35, 5006–5016.
585 Wang, Y.J., Kharaghani, A., Metzger, T., Tsotsas, E., 2012. Pore network drying model for
586 particle aggregates: assessment by X-ray microtomography. Drying Technology 30,
587 1800-1809.
588 Vaquiro, H.A., Clemente, G., Garcia Perez, J.V., Mulet, A., Bon, J., 2009. Enthalpy driven
589 optimization of intermittent drying of Mangiferaindica L., Chemical Engineering
590 Research and Design 87, 885-898.
591 Zhang, J., Datta, A.K., 2004. Some considerations in modeling of moisture transport in heating
592 of hygroscopic materials. Drying Technology 22, 1983-2008.

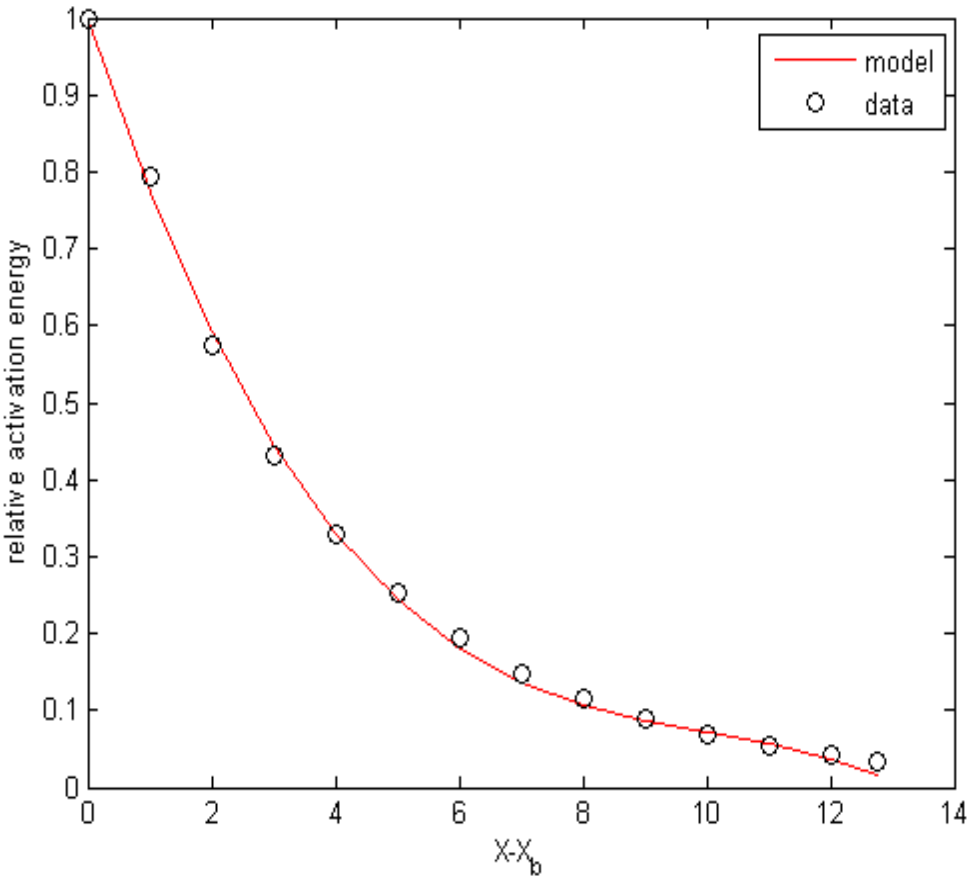
model
data
relative activation energy
X-X$_b$
0
0.1
0.2
0.3
0.4
0.5
0.6
0.7
0.8
0.9
1
0
2
4
6
8
10
12
14

Figure 1. The relative activation energy of eggplant during convective drying at drying air temperature of 60 °C

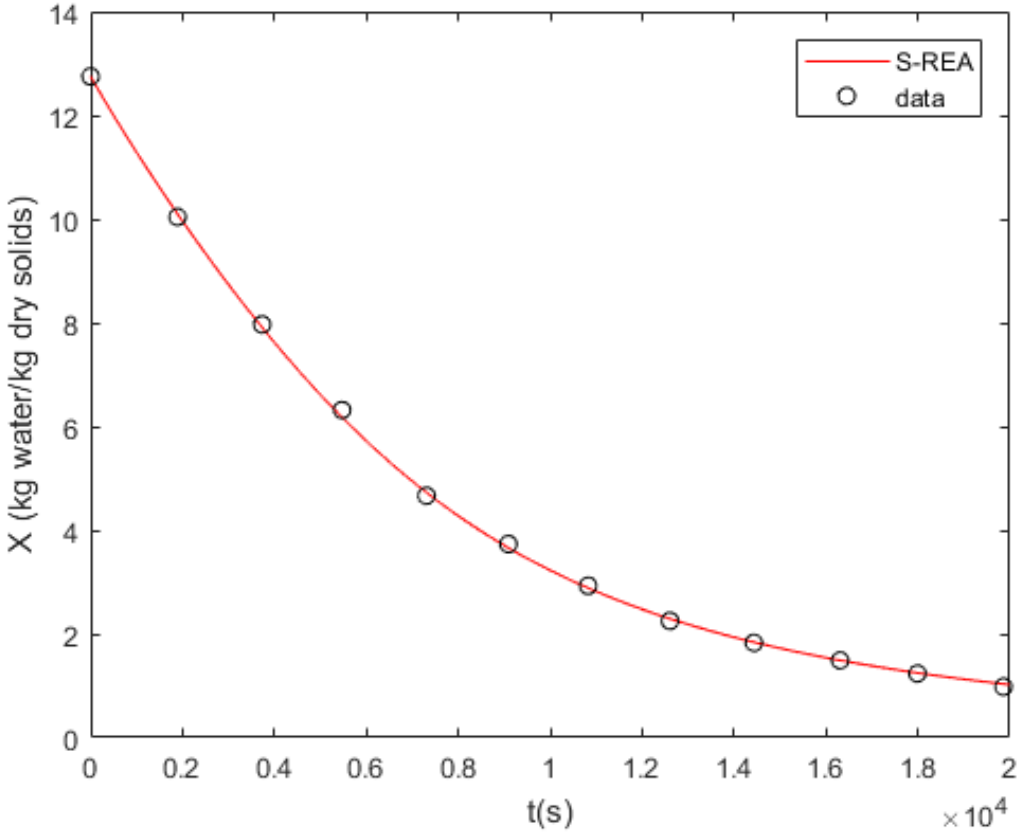

Figure 2. The average moisture content during convective drying at drying air temperature of 50 °C

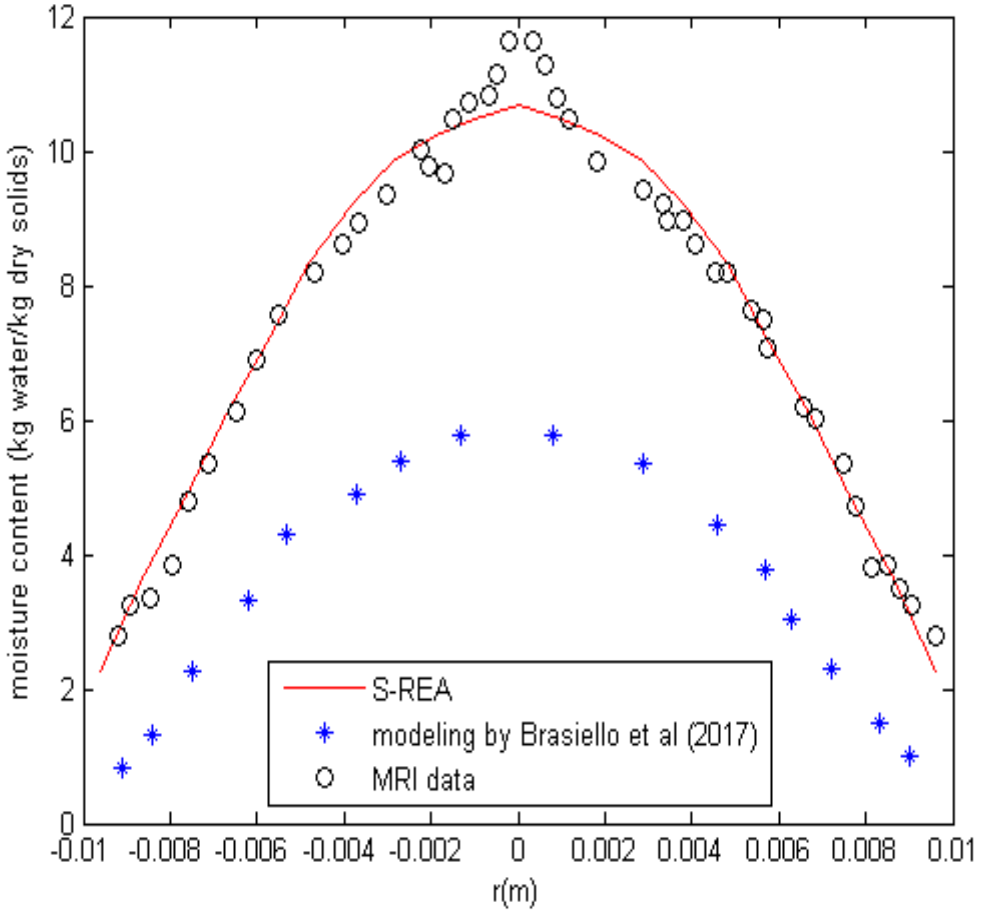

Figure 3. The internal moisture content profiles during convective drying of eggplant at drying time of 1800 s

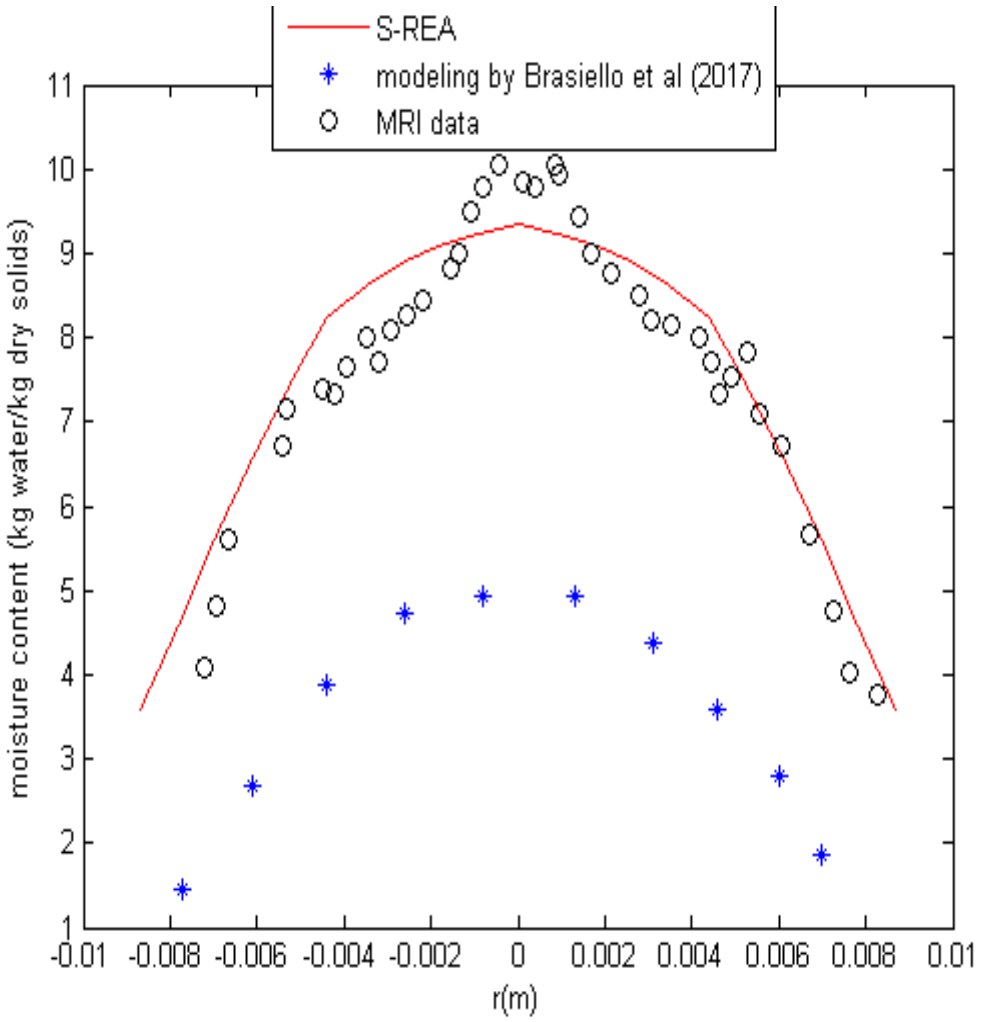
S-REA
modeling by Brasiello et al (2017)
MRI data
moisture content (kg water/kg dry solids)
r(m)
11
10
9
8
7
6
5
4
3
2
1
-0.01
-0.008
-0.006
-0.004
-0.002
0
0.002
0.004
0.006
0.008
0.01

Figure 4. The internal moisture content profiles during convective drying of eggplant at drying time of 3600 s

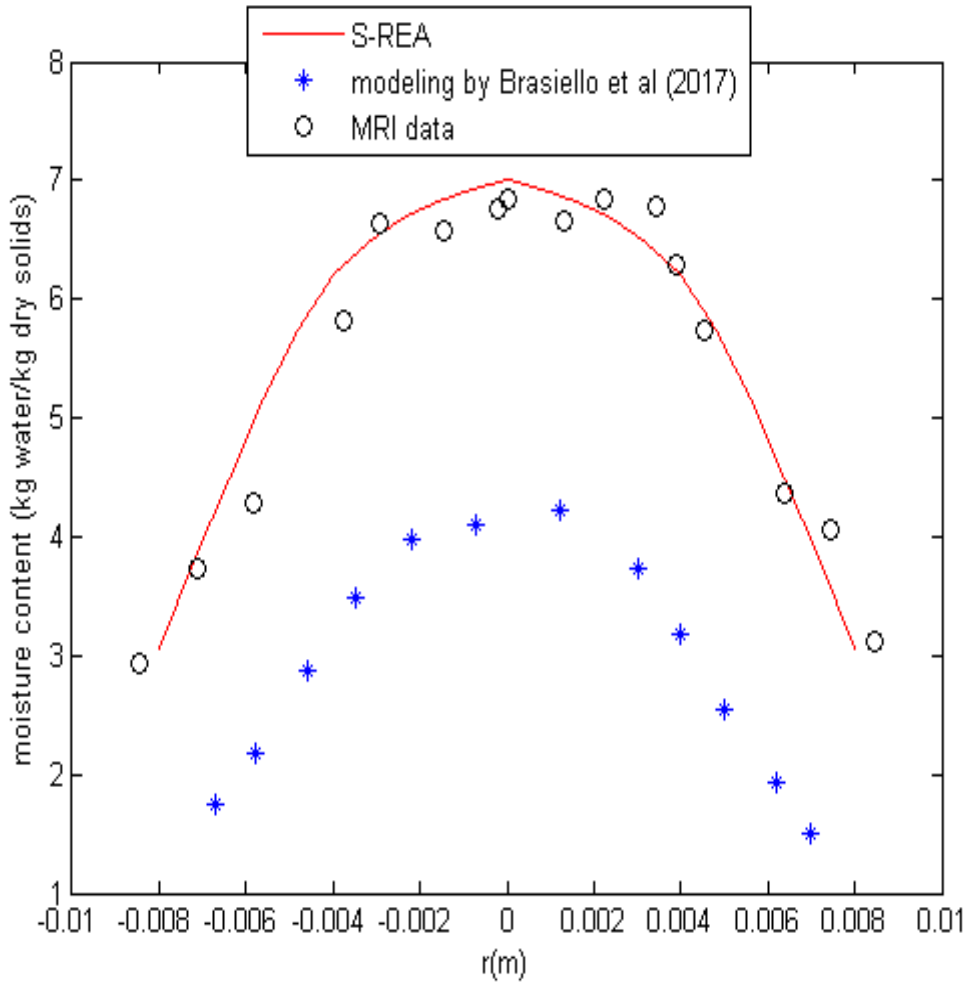

Figure 5. The internal moisture content profiles during convective drying of eggplant at drying time of 5400 s

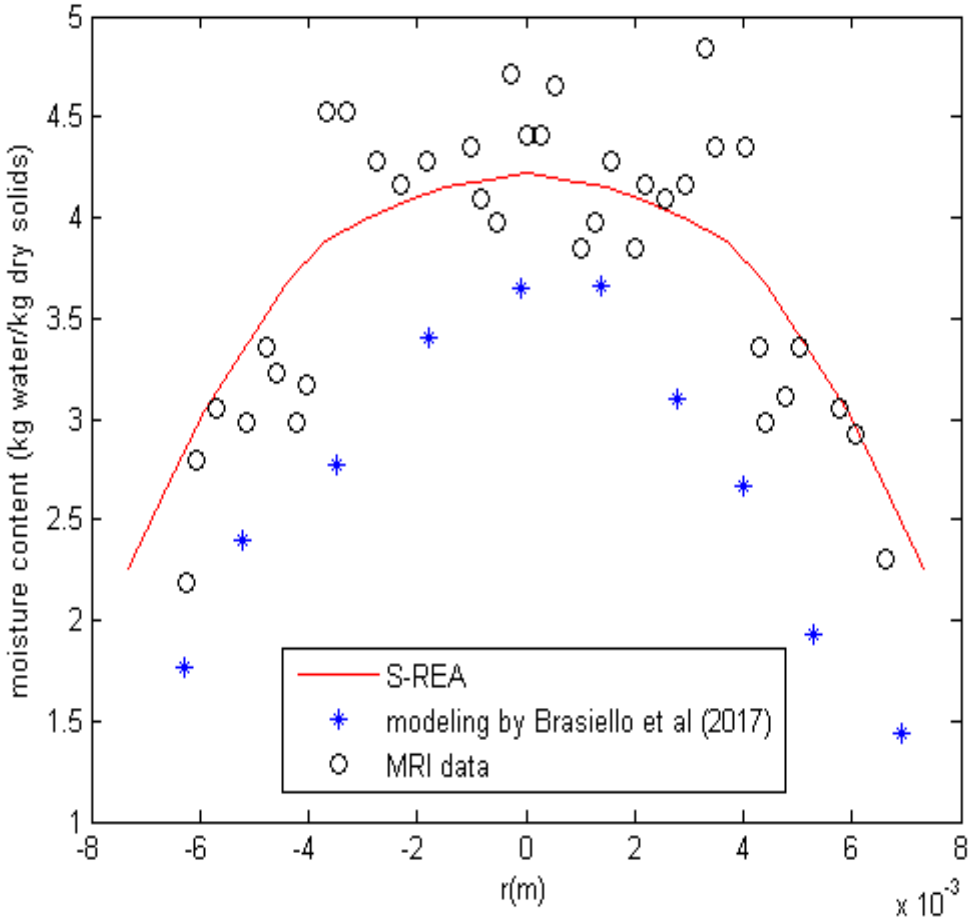

Figure 6. The internal moisture content profiles during convective drying of eggplant at drying time of 7200 s

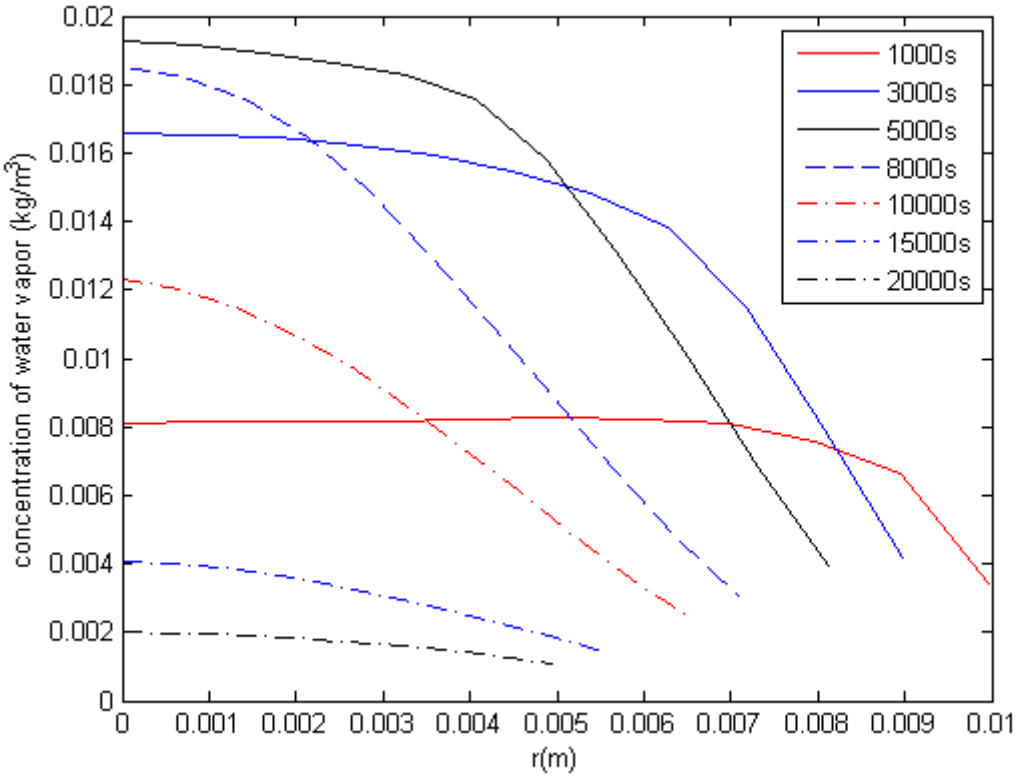

Figure 7. The spatial profiles of concentration of water vapor during convective drying of eggplant at drying air temperature of 50 °C

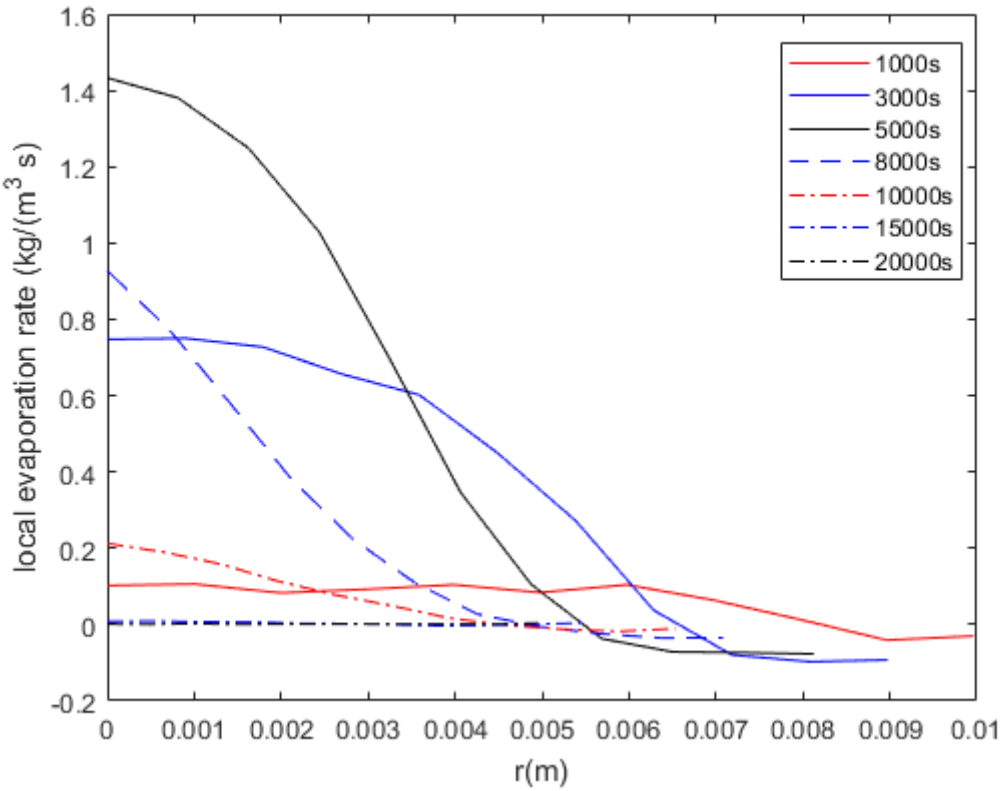

Figure 8. The spatial profiles of local evaporation rate convective drying of eggplant at drying air temperature of 50 °C

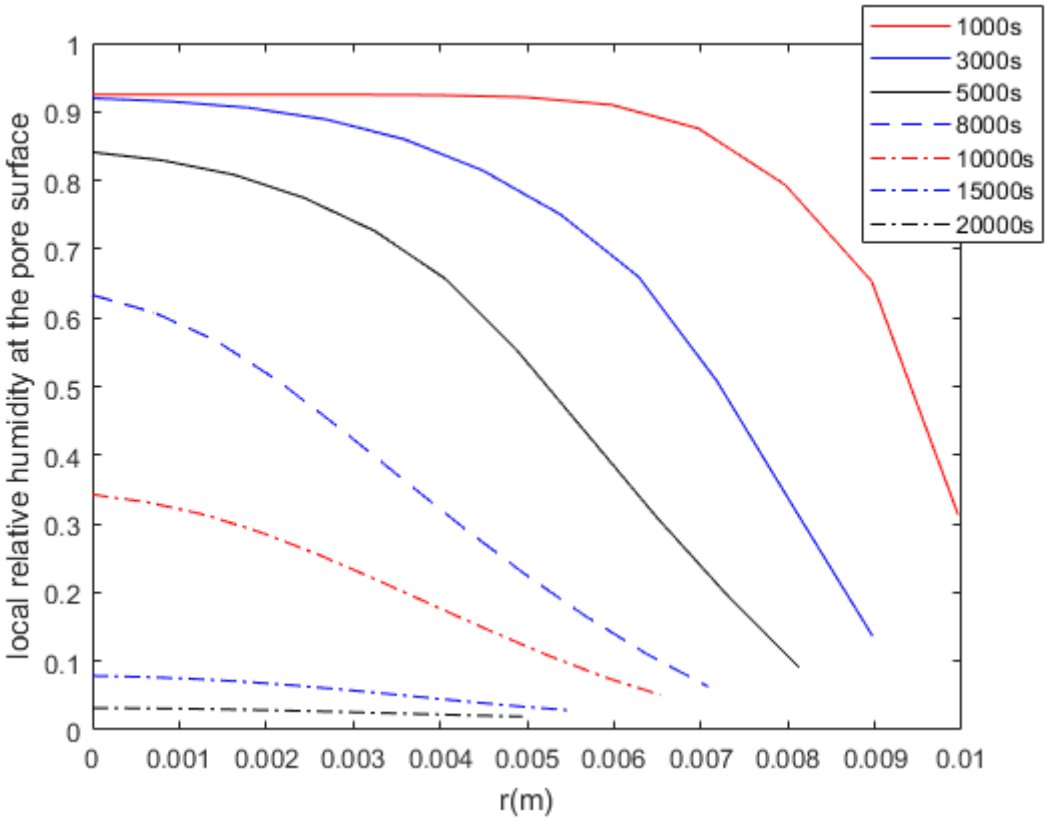

Figure 9. The spatial profiles of local pore surface relative humidity during convective drying of eggplant at drying air temperature of 50 °C

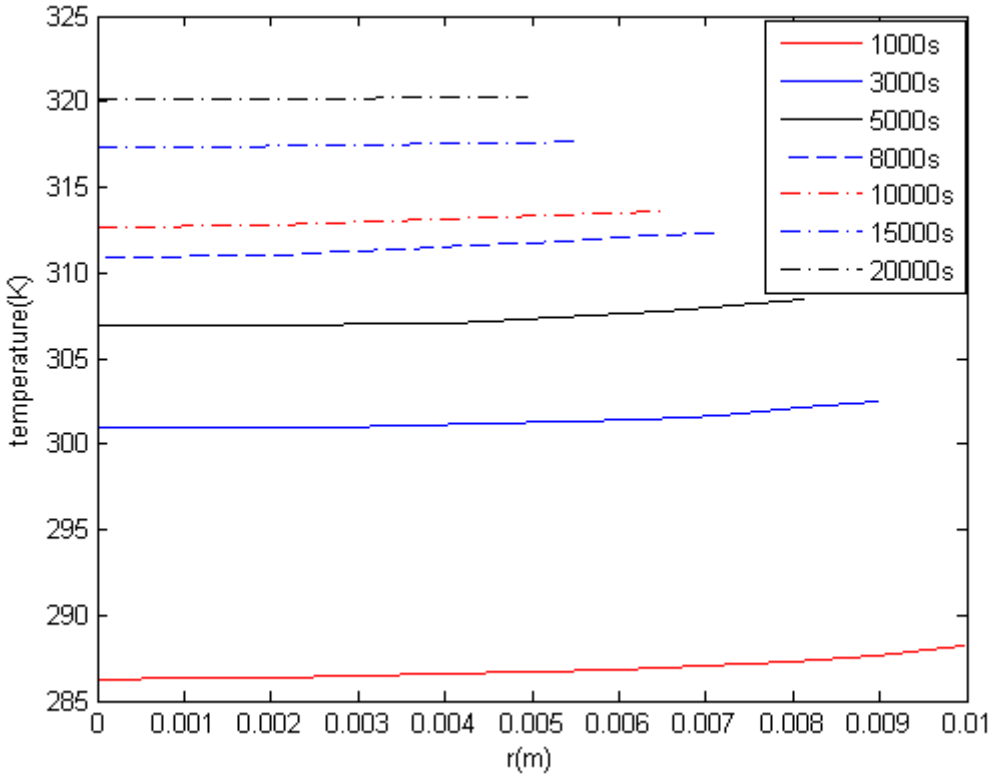

Figure 10. The spatial profiles of temperature during convective drying of eggplant at drying air temperature of 50 °C